

# *Decoupled freshwater transport and meridional overturning in the South Atlantic*

Article

Published Version

Creative Commons: Attribution-Noncommercial-No Derivative Works 4.0

Open Access

Mignac, D., Ferreira, D. ORCID: <https://orcid.org/0000-0003-3243-9774> and Haines, K. ORCID: <https://orcid.org/0000-0003-2768-2374> (2019) Decoupled freshwater transport and meridional overturning in the South Atlantic. *Geophysical Research Letters*, 46 (4). pp. 2178-2186. ISSN 0094-8276 doi: 10.1029/2018GL081328 Available at <https://centaur.reading.ac.uk/82184/>

It is advisable to refer to the publisher's version if you intend to cite from the work. See [Guidance on citing](#).

To link to this article DOI: <http://dx.doi.org/10.1029/2018GL081328>

Publisher: American Geophysical Union

All outputs in CentAUR are protected by Intellectual Property Rights law, including copyright law. Copyright and IPR is retained by the creators or other copyright holders. Terms and conditions for use of this material are defined in the [End User Agreement](#).

[www.reading.ac.uk/centaur](http://www.reading.ac.uk/centaur)

**CentAUR**

Central Archive at the University of Reading

Reading's research outputs online

# Geophysical Research Letters



## RESEARCH LETTER

10.1029/2018GL081328

### Key Points:

- Atlantic overturning freshwater transport is explained by spatial variation in the vertical salinity contrasts between the AMOC branches
- Negligible South Atlantic vertical salinity contrasts produce weak freshwater transports, decoupled from the AMOC strength
- Gyre-driven freshwater transports depend on 0–300 m zonal salinity contrasts and determine the total South Atlantic freshwater transports

### Supporting Information:

- Supporting Information S1
- Table S1

### Correspondence to:

D. Mignac,  
d.mignaccarneiro@pgr.reading.ac.uk

### Citation:

Mignac, D., Ferreira, D., & Haines, K. (2019). Decoupled freshwater transport and meridional overturning in the South Atlantic. *Geophysical Research Letters*, 46, 2178–2186. <https://doi.org/10.1029/2018GL081328>

Received 14 NOV 2018

Accepted 10 FEB 2019

Accepted article online 13 FEB 2019

Published online 25 FEB 2019

## Decoupled Freshwater Transport and Meridional Overturning in the South Atlantic

D. Mignac<sup>1</sup> , D. Ferreira<sup>1</sup> , and K. Haines<sup>2</sup>
<sup>1</sup>Department of Meteorology, University of Reading, Reading, UK, <sup>2</sup>Department of Meteorology and National Centre for Earth Observation, University of Reading, Reading, UK

**Abstract** Freshwater transports ( $F_{ov}$ ) by the Atlantic meridional overturning circulation (AMOC) are sensitive to salinity distributions and may determine AMOC stability. However, climate models show large salinity biases, distorting the relation between  $F_{ov}$  and the AMOC. Using free-running models and ocean reanalyses with realistic salinities but quite different AMOCs, we show that the fresh Antarctic Intermediate Water layer eliminates salinity differences across the AMOC branches at  $\sim 1,200$  m,  $\Delta S_{1200m}$ , which decouples  $F_{ov}$  from the AMOC south of  $\sim 10^\circ\text{N}$ . As the Antarctic Intermediate Water disappears north of  $\sim 10^\circ\text{N}$ , a large  $\Delta S_{1200m}$  allows the AMOC to drive substantial southward  $F_{ov}$  in the North Atlantic. In the South Atlantic the 0–300 m zonal salinity contrasts control the gyre freshwater transports  $F_{gyre}$ , which also determine the total freshwater transports. This decoupling makes the southern  $F_{ov}$  unlikely to play any role in AMOC stability, leaving indirect  $F_{gyre}$  feedbacks or  $F_{ov}$  in the north, as more relevant factors.

**Plain language summary** The Atlantic Ocean has an upper circulation branch transporting warm waters toward the Arctic. These waters sink due to changes in both salinity and temperature, leading to a cold and deep southward circulation branch throughout the Atlantic. This “overturning circulation” moves heat and freshwater over large distances, contributing to regulate Earth’s climate, but the circulation strength may also be affected by these transports via feedback effects. It has been proposed that South Atlantic freshwater transports are a sensitive indicator of circulation feedback, which could lead to instability in the climate system. However, models of the ocean and atmospheric circulations used to study climate often show large errors in salinity distributions and freshwater transports and therefore may misrepresent climate stability. We show that with realistic salinities, the overturning circulation produces virtually no freshwater transports throughout the South Atlantic and is unlikely to have any role in feedbacks causing climate instability. Horizontal gyre circulations dominate South Atlantic freshwater transports, which could still have some indirect influence on climate stability. In contrast, the overturning circulation does drive a strong freshwater transport in the North Atlantic, and therefore, salinity feedbacks on the climate stability are much more likely to be important in the north.

## 1. Introduction

The Atlantic meridional overturning circulation (AMOC) is a key contributor in the global climate system, transporting warm water northward throughout the Atlantic to compensate for the southward export of the cold North Atlantic Deep Water (NADW). In modeling studies an AMOC collapse has been shown to cause severe regional climate changes, such as a surface air temperature cooling of up to  $10^\circ\text{C}$  in the North Atlantic (Jackson et al., 2015; Laurian et al., 2009; Vellinga & Wood, 2002). Global impacts of an AMOC slowdown include a southward shift of the Intertropical Convergence Zone (ITCZ) over the Atlantic and Pacific, as well as in weakened Indian and Asian summer monsoons (Broccoli et al., 2006; Manabe & Stouffer, 1993; Zhang & Delworth, 2005).

The freshwater transport by the AMOC itself ( $F_{ov}$ ) has been proposed as an indicator of the AMOC bistability, a situation where the AMOC could switch between “on” and “off” states (a collapsed or weak AMOC). Based on results from simple box models (De Vries & Weber, 2005; Rahmstorf, 1996; Stommel, 1961), a bistable AMOC is suggested to occur when the overturning circulation exports freshwater from the Atlantic ( $F_{ov} < 0$ ), with  $F_{ov}$  typically being measured at the southern boundary at  $34^\circ\text{S}$ . In this scenario, *assuming other feedbacks are negligible*, a weakening of the AMOC is followed by a weakening of  $F_{ov}$  and freshening of the whole basin, which in turn further reduces the model AMOC, creating a positive feedback loop (Drijfhout et al., 2011; Hawkins et al., 2011).

©2019. The Authors.

This is an open access article under the terms of the Creative Commons Attribution-NonCommercial-NoDerivs License, which permits use and distribution in any medium, provided the original work is properly cited, the use is non-commercial and no modifications or adaptations are made.

However,  $F_{ov}$  at 34°S may be a poor indicator of the true freshwater feedbacks during a changing AMOC, because the South Atlantic subtropical gyre (SASG) can adjust in conjunction with the AMOC, as noted by Sijp (2012). Furthermore,  $F_{ov}$  has also been shown to be sensitive to biases in coupled climate models, with suggested implications that many models may be artificially stable (Jackson, 2013; Liu et al., 2017; Mecking et al., 2017; Yin & Stouffer, 2007). In particular,  $F_{ov}$  in the southern Atlantic can easily change sign when salinity bias corrections are accounted for, as seen for many Coupled Model Intercomparison Project (CMIP5) models (Mecking et al., 2017).

It is in this context that ocean reanalyses (ORAs) can be useful tools to investigate the freshwater transport throughout the Atlantic, since they employ data assimilation (DA) methods to constrain models to a diverse network of available ocean observations, giving a consistent estimate of the historical ocean state (e.g., Masina et al., 2015; Palmer et al., 2015). The complete, time-evolving ORA descriptions of the ocean circulation are already used for initializing climate model transports, aiming to improve decadal predictions of the AMOC (Bellucci et al., 2013; Pohlmann et al., 2009). Comparisons between ORAs and historical model runs without DA, that is, free-running models (FRMs), also give valuable insights into how ocean transports, which are not directly observed, are affected by DA (e.g., Karspeck et al., 2015; Mignac et al., 2018).

In order to elucidate feedbacks between salinity and the strength of the AMOC, here we use two FRMs and four ORAs to investigate the role of salinity in modulating both overturning and gyre freshwater transports across the Atlantic. We also draw some useful comparisons between the meridional freshwater transports and the meridional heat transports. The paper begins with a brief overview of the data set configurations and mathematical framework in sections 2 and 3, respectively. The components of the transports are investigated in section 4, followed by an analysis of the salinity distribution and its impact on the overturning (section 5) and gyre (section 6) freshwater components. Discussion and conclusions are presented in section 7.

## 2. The Data Set

Two FRMs and four ORAs, each with a global domain, are configured with the Nucleus for European Modelling of the Oceans (NEMO; Madec, 2008) model, using a partial cell topography scheme (Adcroft et al., 1997) and a quasi-isotropic tripolar ORCA grid (Madec & Imbard, 1996). The FRMs are referred to here as FRM4 (Haines et al., 2012) and FRM12 (Marzocchi et al., 2015), to distinguish their horizontal resolution of 1/4° and 1/12°, respectively. All the ORAs, produced during the spin-up of the Copernicus Marine service, have eddy-permitting resolution at 1/4°, namely, the European Centre for Medium-Range Weather Forecasts Ocean Reanalysis Pilot 5 (ORAP5; Zuo et al., 2015), the Global Ocean Reanalysis System Version 5 (CGLORSV5; Storto & Masina, 2016), the University of Reading Reanalysis Version 4 (UR025.4; Valdivieso et al., 2014), and the Global Ocean Reanalysis and Simulation Version 4 (GLORYS2V4; CMEMS, 2017). These ORAs employ different state-of-the-art DA schemes (Table S1 in the supporting information) to assimilate a broad range of reprocessed in situ and remotely sensed observations of sea surface temperature, sea surface height, sea ice, temperature, and salinity profiles.

Most of the products are configured with 75  $z$  levels, except FRM4 and CGLORSV5 with 46 and 50  $z$  levels, respectively. All models are forced with ERA-Interim atmospheric fields (Simmons et al., 2007), except FRM12, which employs the DRAKKAR Surface Forcing 4.1 (Brodeau et al., 2010), based on modified ERA-Interim. The FRMs apply a moderate sea surface salinity (SSS) restoring based on Levitus et al. (1998), whereas ORAP5 and CGLORSV5 restore the SSS toward the World Ocean Atlas 2009 (Locarnini et al., 2010) and UK MetOffice EN4.2.1 (Good et al., 2013), respectively. No SSS relaxation has been used in UR025.4 and GLORYS2V4, and the only salinity restoring mechanism is through the DA increments. More details comparing these FRMs and ORAs can be found in Table S1 and in Mignac et al. (2018).

## 3. Mathematical Framework

In order to calculate transports across each latitudinal section, following a number of earlier studies, notably Bryden and Imawaki (2001), the mean baroclinic freshwater and heat transports are decomposed into a mean vertical (overturning) and mean horizontal (gyre) component:

$$F_{mean} = F_{ov} + F_{gyre} = -\frac{1}{\bar{S}} \int v^* \langle S \rangle dz - \frac{1}{\bar{S}} \iint v'' s'' dx dz, \quad (1)$$

$$Q_{mean} = Q_{ov} + Q_{gyre} = \rho C_p \int v^* \langle T \rangle dz + \rho C_p \iint v'' T'' dx dz, \quad (2)$$

where  $\langle \cdot \rangle$  represents the zonal mean, the double prime  $''$  denotes deviations from zonal averages,  $\bar{S}$  is the section averaged salinity, and  $v^*$  corresponds to deviations of the zonal mean meridional velocity from its section averaged values. In equation (2),  $\rho$  is the seawater density ( $\sim 1,025 \text{ kg/m}^3$ ), and  $C_p$  is the specific heat capacity of seawater ( $\sim 4,000 \text{ J}\cdot\text{kg}^{-1}\cdot^\circ\text{C}^{-1}$ ).

Because the UR025.4 product ends in 2010, and to avoid any dynamical spin-up in the early simulation years for GLORYS2V4 starting in 1995, a common time period from 1997 to 2010 is chosen to calculate the mean freshwater and heat transport components for all products.

#### 4. Transport Components

In Figures 1a–1c, the 1997–2010  $F_{mean}$  transports are shown with  $F_{ov}$  and  $F_{gyre}$  components. The gyre component of these transports is antisymmetric with similar magnitudes but opposite sign around  $\sim 5^\circ\text{N}$ , and we will return to this component later. Unlike  $F_{gyre}$ ,  $F_{ov}$  magnitudes are quite different in each hemisphere. Throughout the South Atlantic,  $F_{ov}$  is consistently small, although not consistently negative, ranging from  $-0.07$  to  $0.1 \text{ Sv}$ , and therefore,  $F_{mean}$  is determined by  $F_{gyre}$ . All the products show a slightly negative  $F_{ov}$  at  $34^\circ\text{S}$ , supported by observations (Garzoli et al., 2013), which has been suggested to indicate a bistable AMOC as discussed in section 1. In contrast, the North Atlantic has a large negative  $F_{ov}$  peak reaching  $-0.6 \text{ Sv}$  in the ORAs, also consistent with the observations (McDonagh et al., 2010, 2015). As a result,  $F_{mean}$  is negative through the North Atlantic at least down to  $20^\circ\text{N}$ , due to the dominance of  $F_{ov}$  over  $F_{gyre}$  in the subtropics. The North Atlantic negative  $F_{ov}$  peak in the FRMs is only about  $-0.3 \text{ Sv}$ , consistent with the fresh FRM bias, which will be discussed later.

Figure 1b also clearly shows consistency between the ORAs in reproducing  $F_{ov}$  in both hemispheres, despite AMOC differences of up to  $\sim 6 \text{ Sv}$  at  $34^\circ\text{S}$  and  $26.5^\circ\text{N}$  (Table S1). This is perhaps surprising, as the spread of the ORA mean heat transport  $Q_{mean}$  (Figure 1d) is clearly governed by the spread in the overturning heat component  $Q_{ov}$  (Figure 1e). The gyre heat transports  $Q_{gyre}$  (Figure 1f) are now much smaller in both basins and are also consistent with each other and with the observations, as discussed in Mignac et al. (2018).

#### 5. $F_{ov}$ and Vertical Salinity Structure

The AMOC stream function shown in Figure 2a transports freshwater northward or southward, depending upon the salinity difference between its northward-moving upper branch and its southward-moving lower branch (NADW). Figure 2b shows the zonal- and depth-averaged salinity difference between the upper and lower waters,  $\Delta S$ , as a function of latitude for the FRMs, ORAs, and EN4.2.1. Note that a positive  $\Delta S$  (i.e., upper branch saltier than the lower branch) corresponds to a northward salt transport and a southward freshwater transport (and vice versa). The solid lines correspond to the case where the boundary between upper and lower waters is set at  $1,200 \text{ m}$ ,  $\Delta S_{1200\text{m}}$ , approximately separating the upper and lower AMOC branches (i.e., the depth of the maximum AMOC stream function; Figure 2a). Dashed lines have a dividing boundary at only  $300 \text{ m}$ ,  $\Delta S_{300\text{m}}$ , chosen to match the shallow salinity stratification in the South Atlantic. For the AMOC depth,  $\Delta S_{1200\text{m}}$  is  $\sim 0.8 \text{ psu}$  in the North Atlantic, but this falls to  $\sim 0 \text{ psu}$  in the South Atlantic. Therefore, because the upper and lower branches of the AMOC have similar salinity in the South Atlantic, the AMOC has very little freshwater transports in this basin (Figure 1b), even though the AMOC itself is strong (Figure 2a) and varies greatly between the different products (Table S1). This decoupling between the AMOC and  $F_{ov}$  in the South Atlantic, due to a small  $\Delta S_{1200\text{m}}$ , contrasts with the large North Atlantic  $\Delta S_{1200\text{m}}$  and substantial  $F_{ov}$  between  $20^\circ\text{N}$  and  $40^\circ\text{N}$ .

Figure 2c shows the equivalent temperature differences, with  $\Delta T_{1200\text{m}}$  steady at  $\sim 6^\circ\text{C}$  in the South Atlantic, allowing the AMOC to still play a leading role in heat transport throughout this basin (Figure 1e). Furthermore, the wind-driven subtropical cells (STCs; Zhang et al., 2003), which counteract (enhance) the AMOC south (north) of the equator in Figure 2a, produce a sharp cross-equatorial  $Q_{ov}$  increase but have little effect on  $F_{ov}$  (Figure 1b). Following the same approach as in Figure 2, the  $\Delta S_{1200\text{m}}$  between the



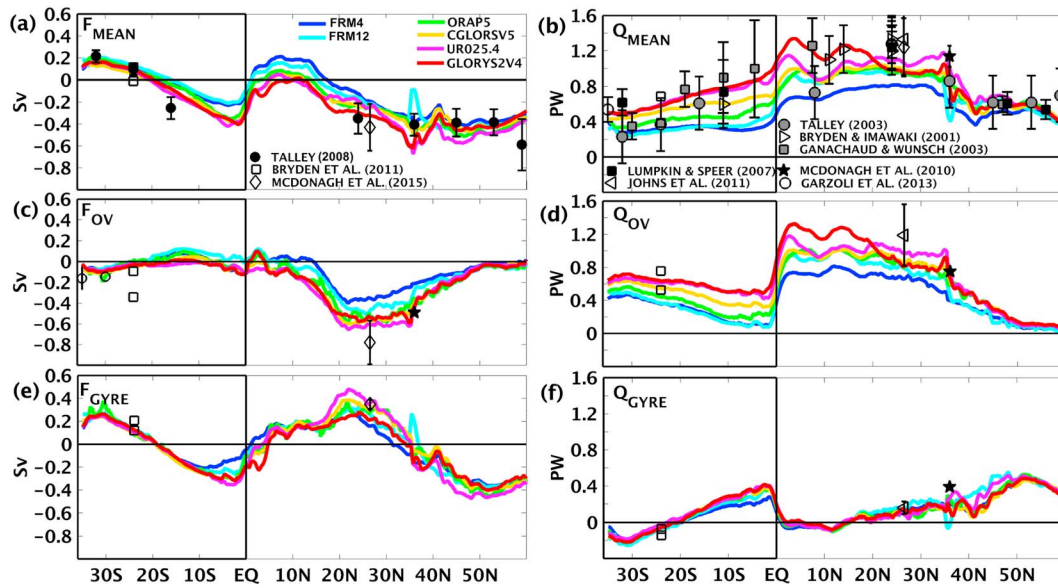


**Figure 1.** The mean (a) freshwater (Sv) and (d) heat transports (PW) across the Atlantic from 1997 to 2010, with their (b and e) overturning and (c and f) gyre components, respectively. Observational transport estimates at various sections are also included for comparison, using calculations based on equations (1) and (2).

upper (0–150 m) and lower (150–300 m) STC branches is less than  $\sim 0.1$  psu (see Figure S1a), which acts to neutralize the STC circulation impact on  $F_{ov}$ . Unlike  $\Delta S_{150m}$ , the  $\Delta T_{150m}$  is  $\sim 8.2$  and  $\sim 8.8$  °C in the south and north STC cells, respectively (Figure S1b), allowing these shallow circulations to contribute significantly to  $Q_{ov}$  near the equator.

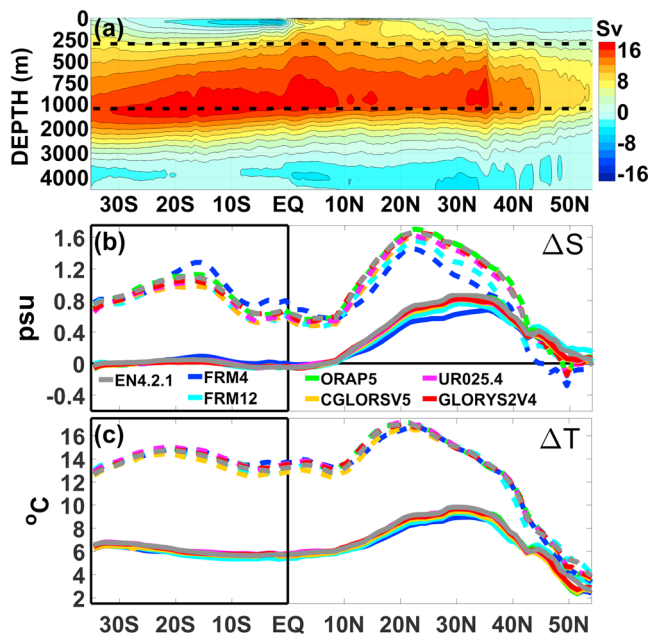


**Figure 2.** (a) The 1997–2010 Atlantic meridional overturning circulation stream function (Sv) computed as the mean of all the model products. In (b) and (c) the 1997–2010 zonally averaged  $\Delta S$  (psu) and  $\Delta T$  (°C) are divided at 300 m (dashed lines) and 1,200 m (solid lines), respectively, to separate the upper and lower branches. The horizontal black dashed lines in (a) correspond to depths of 300 and 1,200 m shown in (b) and (c). Note the stretched vertical axis in (a) between 0 and 1,000 m, compared to 1,000 and 5,000 m.

In order to understand the vertical salinity differences between the northern and southern basins, Figure 3a shows the zonally averaged salinity from EN4.2.1 with superimposed AMOC stream function contours from Figure 2a. The upper ocean salinity maximum in the SASG is weaker and decreases rapidly with depth compared to the North Atlantic Subtropical Gyre (NASG), as seen in Figure 2b. This is partly due to the very fresh Antarctic Intermediate Water (AAIW) formed at  $\sim 50^\circ\text{S}$ , which subducts under the SASG truncating the salinity core to much shallower depths. This intermediate layer is even fresher than the NADW, so that the top 1,200-m layer has almost the same salinity as the NADW below (Figure 3b), giving negligible  $\Delta S_{1200m}$  up to  $\sim 10^\circ\text{N}$  where the AAIW is curtailed. The surface salty core also weakens at the latitude of the mean ITCZ ( $\sim 5^\circ\text{N}$ ), producing a subsurface salinity maximum before it freshens again down to 300 m. This low-high-low salinity structure in the top 300 m near the equator is consistent with the very small  $\Delta S_{150m}$  across the STCs (Figure S1a).

$\Delta S_{1200m}$  increases in the North Atlantic as the AAIW is replaced by the very salty Mediterranean water (MW). The MW helps to deepen and intensify the NASG upper layer salinity core (Blanke et al., 2006; Jia et al., 2007), giving high salinity down to considerable depth in the profiles of Figure 3c. The deep NASG salinity core leads to a strong contrast between the upper and lower layer salinities (i.e., larger  $\Delta S_{1200m}$ ), which then allows the AMOC to produce a strong freshwater transport in the subtropical North Atlantic. The  $F_{ov}$  strength, and hence the coupling between the AMOC and the freshwater budget, is controlled by  $\Delta S_{1200m}$ . This explains key results related to AMOC bistability arguments, for example, how correcting the model salinity biases significantly change

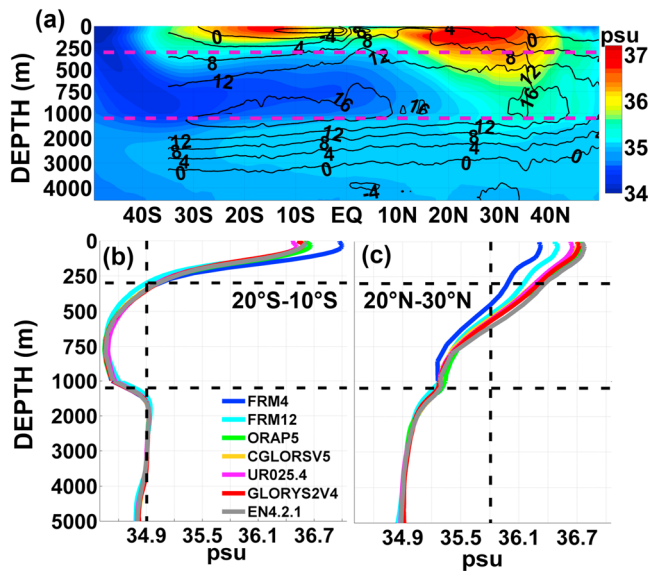


**Figure 3.** (a) The 1997–2010 zonally averaged salinity (psu) from EN4.2.1 in the Atlantic, superimposed with the Atlantic meridional overturning circulation stream function (Sv) contours from Figure 2a. The salinity profiles (psu) from (b) 20°S to 10°S and (c) 20°N to 30°N are also shown for all products. The vertical black dashed lines in (b) and (c) correspond to the 0–1200 m mean salinity from EN4.2.1. The depths of 300 and 1,200 m are represented by the horizontal purple and black dashed lines in (a) and (b) and (c), respectively. Note the stretched vertical axis.

the correlations between the AMOC strength and  $F_{ov}$  through the basin (Mecking et al., 2017).

All the reanalyses show very good agreement with EN4.2.1 salinities in both South and North Atlantic (Figures 2b, 3b, and 3c), due to the assimilation of salinity profiles and the additional SSS relaxation toward climatology in ORAP5 and CGLORSV5. The realistic zonal-depth mean salinities seen in the ORAs in both hemispheres also lead to their consistent  $F_{ov}$  (Figure 1b). The ORAs have larger  $\Delta S_{1200m}$  in the North Atlantic, in better agreement with EN4.2.1 than the FRMs, leading to a larger negative  $F_{ov}$  peak there, which is closer to hydrographic inverse estimates (Figure 1b). The FRM upper layers (0–1200 m), even with SSS restoring, are fresher than EN4.2.1 in the NASG. This is a common model deficiency possibly due to excessive MW mixing with surrounding water masses (Jia, 2000; Jia et al., 2007; Legg et al., 2009), which DA helps to mitigate in the ORAs (Figure 3c). This upper fresh bias reduces the FRM vertical salinity contrasts in the subtropical North Atlantic, giving their smaller negative  $F_{ov}$  peak. In the SASG (Figure 3b) the FRM biases are mostly confined to the top 250 m and therefore project less onto the AMOC upper branch, supporting the better  $F_{ov}$  agreement between all model products in the South Atlantic.

## 6. $F_{gyre}$ and Horizontal Salinity Gradients

We have seen how the shallower (deeper) salinity core of the South (North) Atlantic in Figure 3 influences the  $F_{ov}$  strength. We now evaluate

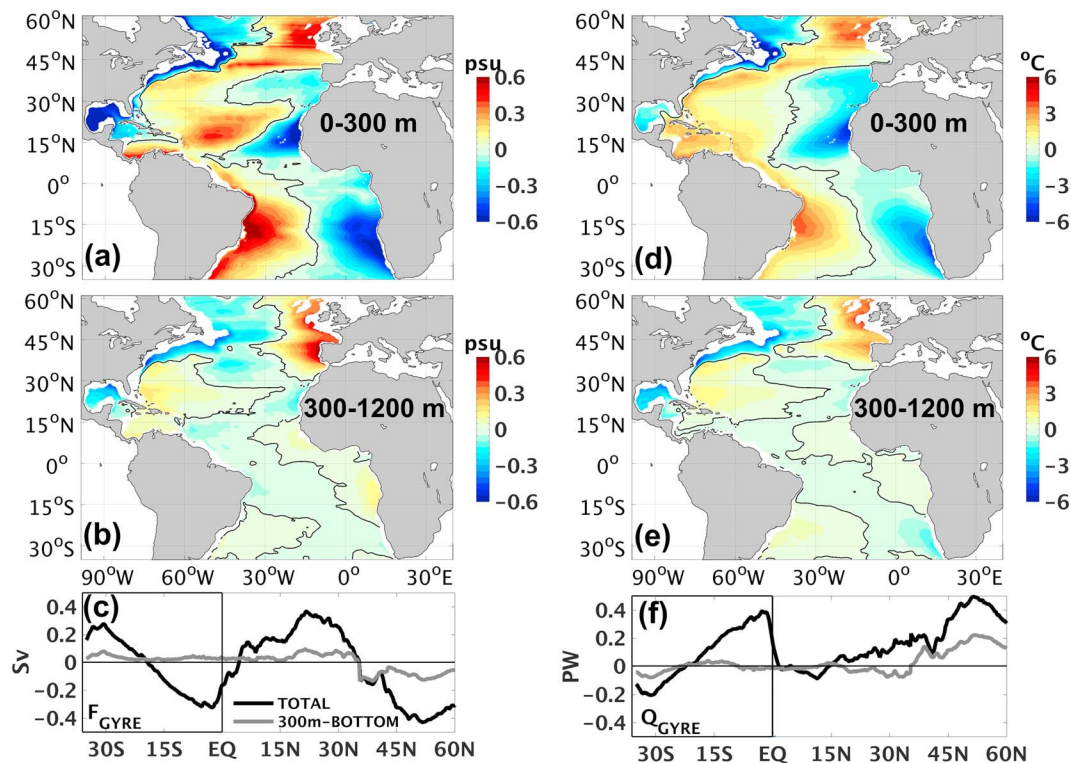


**Figure 4.** The ocean reanalysis depth averaged  $S'$  (a and b) and  $T'$  (d and e) for 0–300 m and 300–1,200 m, respectively. The black solid contour corresponds to 0 psu or 0 °C. The ocean reanalysis meridional gyre freshwater (Sv) and heat (PW) transports are displayed in (c) and (f), respectively, for the total depth (black) and 300 m-bottom (gray).

the salinity and temperature deviations from zonal averages,  $S''$  in equation (1) and  $T''$  in equation (2), for particular depth ranges upon which the gyre circulation acts. Figure 4 shows that  $S''$  and  $T''$  are much stronger in the upper 0–300 m relative to the 300–1200 m depth range in both hemispheres, but especially in the South Atlantic. Although the gyre circulations extend deeper (Figure S2), only the top 300 m makes a significant contribution to the gyre freshwater and heat transports south of 30°N (Figures 4c and 4f), as the zonal salinity and temperature contrasts below 300 m are much smaller (Figures 4b and 4e). North of ~30°N there are still relatively large zonal deviations in the 300–1200 m depth range due to contrasts caused by the Gulf Stream and, on the eastern side, by the injection of the MW outflow at mid-depths. This leads to more significant  $S''$  and  $T''$  contributions to the gyre transports below 300 m. Very similar patterns can also be found in the FRMs (Figure S3).

The gyres in Figure 4c lead to freshwater convergence at ~20°S and ~35°N, acting to balance the positive evaporation minus precipitation at these latitudes. The shallowness of the main  $F_{gyre}$  transports in most of the basin (Figure 4c) is required to compensate for this surface forcing (see Figure S4), which maintains the strong near surface salinity gradients in Figure 3a. This is also consistent with the fact that  $F_{gyre}$  transports in the North Atlantic look quite similar in magnitude to those in the south, with an antisymmetric pattern around the mean ITCZ location at ~5°N (Figure S4).

## 7. Discussion and Conclusions

The ocean transport components, particularly of freshwater, in both South and North Atlantic are investigated in two NEMO FRMs and four ORAs over 1997–2010. We show that variations in the strength of the freshwater overturning transport  $F_{ov}$  through the basin are largely explained by variations of the vertical salinity contrast  $\Delta S_{1200m}$ , based on the separation between the upper and lower AMOC branches at ~1,200 m. South of ~10°N, the very fresh AAIW limits the evaporation-driven high salinity layer to shallower depths. The average salinity through the top 1,200 m is then almost the same as the salinity below 1,200 m consisting mostly of NADW. As a consequence of this small  $\Delta S_{1200m}$ , seen in the FRMs, ORAs, and observations, the AMOC, despite transporting a substantial amount of heat at these latitudes, has only very small freshwater transports. Even the shallow wind-driven STCs, which contribute to the cross-equatorial heat transports, do not add significant freshwater transport to  $F_{ov}$  due to the small  $\Delta S$  between the upper (0–150 m) and lower (150–300 m) STC branches near the equator. North of ~10°N  $F_{ov}$  rapidly increases as the AAIW layer disappears, allowing the development of a substantial vertical salinity contrast between the AMOC branches, especially in the ORAs, and driving large southward freshwater transports in the NASG.

Since a realistic  $\Delta S_{1200m}$  effectively shuts off, or greatly weakens, first-order feedbacks between the AMOC changes and  $F_{ov}$  throughout the South Atlantic, the use of  $F_{ov}$  at 34°S (e.g., Rahmstorf, 1996) as an indicator of the AMOC bistability must be questioned. This feedback relies on  $F_{ov}$  changing with the AMOC strength and acting as the main feedback on the North Atlantic freshwater budget. Our results emphasize that  $F_{ov}$  at 34°S is *not* strongly coupled to the AMOC, nor is it likely to be a significant term in the freshwater budget, at least when compared to northern latitudes where  $F_{ov}$  is nearly an order of magnitude larger.

After correcting the salinity biases in the CMIP5 models, Mecking et al. (2017) found large changes in the correlation patterns between the basin-scale  $F_{ov}$  and the AMOC strength computed at 26.5°N. Correlations based on the modeled salinity fields, which were significantly positive south of ~10°N, become very small after model salinities are corrected (e.g., essentially zero at 34°S). This also shows that with a realistic vertical salinity structure the wide range of AMOC strengths in CMIP5 models have basically no impact on the South Atlantic  $F_{ov}$ . This is consistent with our results: Although the FRMs and ORAs show large AMOC discrepancies (e.g., up to ~8 Sv; see Mignac et al., 2018), they all give a consistently small  $F_{ov}$  throughout the South Atlantic. They all have a weak negative  $F_{ov}$  at 34°S, also seen in the bias-corrected CMIP5 models, but significantly for the bistability argument,  $F_{ov}$  also varies in sign through the South Atlantic (Figure 1b). As shown by our investigation, the decoupling between the AMOC and  $F_{ov}$  exists at all latitudes south of ~10°N due to the negligible  $\Delta S_{1200m}$ , ensuring the very small  $F_{ov}$  throughout the South Atlantic.



The Atlantic vertical salinity distributions, including the water mass formation regions, are unrealistic in many climate models due to poor freshwater flux fields from the atmosphere component. For example, in the majority of the CMIP5 models a fresh surface bias in the AAIW formation region leads to a fresh, less-dense, and shallower AAIW layer throughout the South Atlantic (Sallée et al., 2013; Yin & Stouffer, 2007; Zhu et al., 2018). This fresh upper layer bias leads to a negative  $\Delta S_{1200m}$ , explaining the spurious South Atlantic correlations between  $F_{ov}$  and AMOC strength in the uncorrected CMIP5 models (Mecking et al., 2017). However, there is no reason why these correlated biases between different CMIP5 models would be relevant to stabilizing or destabilizing feedbacks on the AMOC when  $\Delta S_{1200m}$  is  $\sim 0$  psu as in the real system, because there would be no direct mechanism by which an AMOC change could influence the AAIW water formation region and hence move  $\Delta S_{1200m}$  away from  $\sim 0$  psu.

We also show that the freshwater gyre transport  $F_{gyre}$  mostly determines the South Atlantic total transport  $F_{mean}$ . At  $34^\circ S$ ,  $F_{gyre}$  is consistently larger than  $F_{ov}$ , so that the total transport is actually northward and compensates for the net evaporation in the subtropical South Atlantic. These  $F_{gyre}$  transports exhibit a marked antisymmetric pattern around the mean ITCZ location at  $\sim 5^\circ N$ , redistributing freshwater within a 0–300 m upper ocean layer in the subtropics of both hemispheres. In a freshwater hosing experiment with an eddy-permitting coupled model, Mecking et al. (2016) showed that the dominant response of  $F_{gyre}$  at  $\sim 34^\circ S$  is over twice as large as the changes in  $F_{ov}$ , despite the total AMOC collapsed. Changes in evaporation minus precipitation induced by an AMOC collapse, such as an ITCZ shift, also support the large  $F_{gyre}$  changes found by Mecking et al. (2016) in the South Atlantic. Our analysis, combined with previous literature, suggests that feedbacks associated with  $F_{gyre}$  will likely dominate those associated with  $F_{ov}$  throughout the South Atlantic and thus would be more relevant in any AMOC bistability scenario.

Yin and Stouffer (2007) and Mecking et al. (2016) instead suggest that a better bistability indicator might be to measure  $F_{ov}$  across the NASG where the salinity bias-corrected CMIP5 models show the largest correlations between  $F_{ov}$  and AMOC strength (Mecking et al., 2017). Our results identify the substantial  $\Delta S_{1200m}$  in the NASG, particularly in the ORAs, where DA helps to reduce salinity biases, for example, arising due to the excessive mixing of MWs seen in the FRMs. However, applying the same reasoning as for  $F_{ov}$  at  $34^\circ S$  (see section 1), one would conclude that all models are therefore unstable, as they systematically simulate a large negative  $F_{ov}$  in the NASG (see Figure 1b and Mecking et al., 2017). As this does not appear to be the case, it is evident that other feedbacks, oceanic as well as atmospheric, would likely play a significant role in the instance of an AMOC weakening.

## Acknowledgments

All the reanalyses used in this work are available for scientific research and can be downloaded from the following repositories: UR025.4 (<http://dx.doi.org/10.5285/4bcfa3a4-c7ec-4414-863d-caeeb21f16f>), CGLORSV5 (<https://doi.pangaea.de/10.1594/PANGAEA.857995>), GLORYS2V4 ([ftp://rancmems.mercator-ocean.fr/Core/GLOBAL\\_REANALYSIS\\_PHY\\_001\\_025](ftp://rancmems.mercator-ocean.fr/Core/GLOBAL_REANALYSIS_PHY_001_025)), and ORAP5 ([ftp://rancmems.mercator-ocean.fr/Core/GLOBAL\\_REANALYSIS\\_PHYS\\_001\\_017](ftp://rancmems.mercator-ocean.fr/Core/GLOBAL_REANALYSIS_PHYS_001_017)). The last two can be downloaded after the registration in the Copernicus Marine Environment Monitoring Service (<http://marine.copernicus.eu/>). The first author would like to acknowledge the financial support of the CAPES Foundation, Brazil (proc. BEX 1386/15-8). The authors would also like to mention the support of the ORA providers and the Copernicus Marine Service for providing access to the reanalysis data used in this work.

## References

- Adcroft, A., Hill, C., & Marshall, J. (1997). Representation of topography by shaved cells in a height coordinate ocean model. *Monthly Weather Review*, 125(9), 2293–2315.
- Bellucci, A., Gualdi, S., Masina, S., Storto, S., Scoccimarro, E., Cagnazzo, C., et al. (2013). Decadal climate predictions with a coupled AOGCM initialized with oceanic reanalyses. *Climate Dynamics*, 40(5–6), 1483–1497. <https://doi.org/10.1007/s00382-012-1468-z>
- Blanke, B., Arhan, M., & Speich, S. (2006). Salinity changes along the upper limb of the Atlantic thermohaline circulation. *Geophysical Research Letters*, 33, L06609. <https://doi.org/10.1029/2005GL024938>
- Broccoli, A. J., Dahl, K. A., & Stouffer, R. J. (2006). Response of the ITCZ to Northern Hemisphere cooling. *Geophysical Research Letters*, 33, L01702. <https://doi.org/10.1029/2005GL02454>
- Brodeau, L., Barnier, B., Treguier, A.-M., Penduff, T., & Gulev, S. (2010). An ERA40-based atmospheric forcing for global ocean circulation models. *Ocean Modelling*, 31(3–4), 88–104. <https://doi.org/10.1016/j.ocemod.2009.10.005>
- Bryden, H. L., & Imawaki, S. (2001). Ocean heat transport. In G. Siedler, J. Church, & J. Gould (Eds.), *Ocean circulation and climate* (pp. 455–474). London: Academic Press.
- Bryden, H. L., King, A. B., & McCarthy, G. D. (2011). South Atlantic overturning circulation at 24S. *Journal of Marine Research*, 69(1), 38–55. <https://doi.org/10.1357/002224011798147633>
- Copernicus Marine Environmental Monitoring Service (CMEMS). (2017). Product user manual. Retrieved from <http://marine.copernicus.eu/documents/PUM/CMEMS-GLO-PUM-001-025.pdf>
- De Vries, P., & Weber, S. L. (2005). The Atlantic freshwater budget as a diagnostic for the existence of a stable shut down of the meridional overturning circulation. *Geophysical Research Letters*, 32, L09606. <https://doi.org/10.1029/2004GL021450>
- Drijfhout, S. S., Weber, S. L., & van der Waluw, E. (2011). The stability of the MOC as diagnosed from model projections for pre-industrial, present and future climates. *Climate Dynamics*, 37(7–8), 1575–1586. <https://doi.org/10.1007/s00382-010-0930-z>
- Ganachaud, A., & Wunsch, C. (2003). Large scale ocean heat and freshwater transports during the World Ocean Circulation Experiment. *Journal of Climate*, 16, 695–705.
- Garzoli, S. L., Baringer, M. O., Dong, S., Perez, R., & Yao, Q. (2013). South Atlantic meridional fluxes. *Deep-Sea Research Part I*, 71, 21–32. <https://doi.org/10.1016/j.dsr.2012.09.003>
- Good, S. A., Martin, M. J., & Rayner, N. A. (2013). EN4: Quality controlled ocean temperature and salinity profiles and monthly objective analyses with uncertainty estimates. *Journal of Geophysical Research: Oceans*, 118, 6704–6716. <https://doi.org/10.1002/2013JC009067>

- Haines, K., Valdivieso, M., Zuo, H., & Stepanov, V. N. (2012). Transports and budgets in a 1/4° global ocean reanalysis 1989–2010. *Ocean Science*, 8, 333–344. <https://doi.org/10.5194/os-8-333-2012>
- Hawkins, E., Smith, R. S., Allison, L. C., Gregory, J. M., Woolings, T. J., Pohlmann, H., & de Cuevas, B. (2011). Bistability of the Atlantic overturning circulation in a global climate model and links to ocean freshwater transport. *Geophysical Research Letters*, 38, L10605. <https://doi.org/10.1029/2011GL047208>
- Jackson, L. C. (2013). Shutdown and recovery of the AMOC in a coupled global climate model: The role of the advective feedback. *Geophysical Research Letters*, 40, 1182–1188. <https://doi.org/10.1002/grl.50289>
- Jackson, L. C., Kahana, R., Graham, T., Ringer, M. A., Woolings, T., Mecking, J. V., & Wood, R. A. (2015). Global and European climate impacts of a slowdown of the AMOC in a high resolution GCM. *Climate Dynamics*, 45(11–12), 3299–3316. <https://doi.org/10.1007/s00382-015-2540-2>
- Jia, Y. (2000). Formation of an Azores Current due to the Mediterranean overflow in a modeling study of the North Atlantic. *Journal of Physical Oceanography*, 30(9), 2342–2358. [https://doi.org/10.1175/1520-0485\(2000\)030<2342:FOAACD>2.0.CO;2](https://doi.org/10.1175/1520-0485(2000)030<2342:FOAACD>2.0.CO;2)
- Jia, Y., Coward, A. C., De Cuevas, B. A., & Webb, D. J. (2007). A model analysis of the behavior of the Mediterranean water in the North Atlantic. *Journal of Physical Oceanography*, 37(3), 764–786. <https://doi.org/10.1175/JPO3020.1>
- Johns, W. E., Baringer, M. O., Beal, L. M., Cunningham, S. A., Kanzow, T., Bryden, H. L., et al. (2011). Continuous, Array-based estimates of Atlantic Ocean heat transport at 26.5°N. *Journal of Climate*, 24(10), 2429–2449. <https://doi.org/10.1175/2010JCLI3997.1>
- Karspeck, A. R., Stammer, D., Kohl, A., Danabasoglu, G., Balmaseda, M., Smith, D. M., et al. (2015). Comparison of the Atlantic meridional overturning circulation between 1960 and 2007 in six ocean reanalysis products. *Climate Dynamics*, 49(3), 957–982. <https://doi.org/10.1007/s00382-015-2787-7>
- Laurian, A., Drijfhout, S. S., Hazeleger, W., & Hurk, B. (2009). Response of the Western European climate to a collapse of the thermohaline circulation. *Climate Dynamics*, 34, 689–697.
- Legg, S., Briegleb, B., Chang, Y., Chassignet, E. P., Danabasoglu, G., Ezer, T., et al. (2009). Improving oceanic overflow representation in climate models. The Gravity Current Entrainment Climate Process Team. *Bulletin of the American Meteorological Society*, 90(5), 657–670. <https://doi.org/10.1175/2008BAMS2667.1>
- Levitus, S., Boyer, T. P., Conkright, M. E., O'Brien, T., Antonov, J., Stephens, C., et al. (1998). *World Ocean Database 1998, volume 1: Introduction*, NOAA Atlas NESDIS 18 (Technical Report) (p. 251). Washington, DC: U.S. Government Printing Office.
- Liu, W., Xie, S.-P., Liu, Z., & Zhu, J. (2017). Overlooked possibility of a collapsed Atlantic meridional overturning circulation in warming climate. *Science Advances*, 3(1). <https://doi.org/10.1126/sciadv.1601666>
- Locarnini, R., Mishonov, A., Antonov, J., Boyer, T., Garcia, H., Baranova, O., et al. (2010). In S. Levitus (Ed.), *World Ocean Atlas 2009, volume 1: Temperature*, NOAA Atlas NESDIS 68 (Technical Report) (p. 184). Washington, DC: U.S. Government Printing Office.
- Lumpkin, R., & Speer, K. (2007). Global Ocean meridional overturning. *Journal of Physical Oceanography*, 37(10), 2550–2562. <https://doi.org/10.1175/JPO3130.1>
- Madec, G. (2008). NEMO ocean engine. *Note du Pole de modélisation*, Institut Pierre-Simon Laplace (IPSL), France, 27, 1288–1619.
- Madec, G., & Imbard, M. (1996). A global ocean mesh to overcome the North Pole singularity. *Climate Dynamics*, 12(6), 381–388. <https://doi.org/10.1007/BF00211684>
- Manabe, S., & Stouffer, R. J. (1993). Century-scale effects of increased atmospheric CO<sub>2</sub> on the ocean-atmosphere system. *Nature*, 364(6434), 215–218. <https://doi.org/10.1038/364215a0>
- Marzocchi, A., Hirschi, J. J.-M., Holliday, N. P., Cunningham, S. A., Blaker, A. T., & Coward, A. C. (2015). The North Atlantic subpolar circulation in an eddy-resolving global ocean model. *Journal of Marine Systems*, 142, 126–143. <https://doi.org/10.1016/j.jmarsys.2014.10.007>
- Masina, S., Storto, A., Ferry, N., Valdivieso, M., Haines, K., Balmaseda, M., et al. (2015). An ensemble of eddy-permitting global ocean reanalyses from the MyOcean project. *Climate Dynamics*, 49(3), 813–841. <https://doi.org/10.1007/s00382-015-2728-5>
- McDonagh, E. L., King, B. A., Bryden, H. L., Courtois, P., Szuts, Z., Baringer, M., et al. (2015). Continuous estimate of Atlantic oceanic freshwater flux at 26.5°N. *Journal of Climate*, 28(22), 8888–8906. <https://doi.org/10.1175/JCLI-D-14-00519.1>
- McDonagh, E. L., McLeod, P., King, B. A., Bryden, H. L., & Valdés, S. T. (2010). Circulation, heat, and freshwater transport at 36°N in the Atlantic. *Journal of Physical Oceanography*, 40(12), 2661–2678. <https://doi.org/10.1175/2010JPO4176.1>
- Mecking, J. V., Drijfhout, S. S., Jackson, L. C., & Andrews, M. B. (2017). The effect of model bias on Atlantic freshwater transport and implications for AMOC bi-stability. *Tellus A*, 69, 1–14.
- Mecking, J. V., Drijfhout, S. S., Jackson, L. C., & Graham, T. (2016). Stable AMOC off state in an eddy-permitting coupled climate model. *Climate Dynamics*, 47(7–8), 2455–2470. <https://doi.org/10.1007/s00382-016-2975-0>
- Mignac, D., Ferreira, D., & Haines, K. (2018). South Atlantic meridional transports from NEMO-based simulations and reanalyses. *Ocean Science*, 14(1), 53–68. <https://doi.org/10.5194/os-14-53-2018>
- Palmer, M. D., Roberts, C. D., Balmaseda, M., Chang, Y.-S., Chepurin, G., Ferry, N., et al. (2015). Ocean heat content variability and change in an ensemble of ocean reanalyses. *Climate Dynamics*, 49(3), 909–930. <https://doi.org/10.1007/s00382-015-2801-0>
- Pohlmann, H., Jungclauss, J. H., Köhl, A., Stammer, D., & Marotzke, J. (2009). Initializing decadal climate predictions with the GECCO oceanic synthesis: Effects on the North Atlantic. *Journal of Climate*, 22(14), 3926–3938. <https://doi.org/10.1175/2009JCLI2535.1>
- Rahmstorf, S. (1996). On the freshwater forcing and transport of the Atlantic thermohaline circulation. *Climate Dynamics*, 12(12), 799–811. <https://doi.org/10.1007/s003820050144>
- Sallée, J. B., Shuckburgh, E., Bruneau, N., Meijers, A., Wang, Z., & Bracegirdle, T. (2013). Assessment of Southern Ocean water mass circulation in CMIP5 models: Historical bias and forcing response. *Journal of Geophysical Research: Oceans*, 118, 1830–1844. <https://doi.org/10.1002/jgrc.20135>
- Sijp, W. P. (2012). Characterising meridional overturning bistability using a minimal set of state variables. *Climate Dynamics*, 39(9–10), 2127–2142. <https://doi.org/10.1007/s00382-011-1249-0>
- Simmons, A., Uppala, S., Dee, D., & Kobayashi, S. (2007). ERA-interim: New ECMWF reanalysis products from 1989 onwards. *ECMWF Newsletter*, 110, 25–35.
- Stommel, H. M. (1961). Thermohaline convection with two stable regimes of flow. *Tellus*, 13, 224–230.
- Storto, A., & Masina, S. (2016). C-GLORSv5: An improved multipurpose global ocean eddy-permitting physical reanalysis. *Earth System Science*, 8(2), 679–696. <https://doi.org/10.5194/essd-8-679-2016>
- Talley, L. D. (2003). Shallow, intermediate and deep overturning components of the global heat budget. *Journal of Physical Oceanography*, 33(3), 530–560. [https://doi.org/10.1175/1520-0485\(2003\)033<0530:SIADOC>2.0.CO;2](https://doi.org/10.1175/1520-0485(2003)033<0530:SIADOC>2.0.CO;2)

- Talley, L. D. (2008). Freshwater transport estimates and the global overturning circulation: Shallow, deep and throughflow components. *Progress in Oceanography*, 78(4), 257–303. <https://doi.org/10.1016/j.pocean.2008.05.001>
- Valdivieso, M., Haines, K., Zuo, H., & Lea, D. (2014). Freshwater and heat transports from global ocean synthesis. *Journal of Geophysical Research: Oceans*, 119, 394–409. <https://doi.org/10.1002/2013JC009357>
- Vellinga, M., & Wood, R. (2002). Global climate impacts of a collapse of the Atlantic thermohaline circulation. *Climate Change*, 54(3), 251–267. <https://doi.org/10.1023/A:1016168827653>
- Yin, J., & Stouffer, R. J. (2007). Comparison of the stability of the Atlantic thermohaline circulation in two coupled atmosphere-ocean general circulation models. *Journal of Climate*, 20(17), 4293–4315. <https://doi.org/10.1175/JCLI4256.1>
- Zhang, D., McPhaden, M. J., & Johns, W. E. (2003). Observational evidence for flow between the subtropical and tropical Atlantic: The Atlantic tropical cells. *Journal of Physical Oceanography*, 33(8), 1783–1797. <https://doi.org/10.1175/2408.1>
- Zhang, R., & Delworth, T. L. (2005). Simulated tropical response to a substantial weakening of the Atlantic thermohaline circulation. *Journal of Climate*, 18(12), 1853–1860. <https://doi.org/10.1175/JCLI3460.1>
- Zhu, C., Liu, Z., & Gu, S. (2018). Model bias for South Atlantic Antarctic Intermediate Water in CMIP5. *Climate Dynamics*, 50(9–10), 3613–3624. <https://doi.org/10.1007/s00382-017-3828-1>
- Zuo, H., Balmaseda, M. A., & Mogensen, K. (2015). The new eddy-permitting ORAP5 ocean reanalysis: Description, evaluation and uncertainties in climate signals. *Climate Dynamics*, 49(3), 791–811. <https://doi.org/10.1007/s00382-015-2675-1>